LETTERS
PUBLISHED ONLINE: 20 MAY 2012 | DOI: 10.1038/NMAT3335
nature materials

Electrical control of the superconducting-to-insulating transition in graphene–metal hybrids

Adrien Allain, Zheng Han and Vincent Bouchiat*

Graphene[1] is a sturdy and chemically inert material exhibiting an exposed two-dimensional electron gas of high mobility. These combined properties enable the design of graphene composites, based either on covalent[2] or non-covalent[3] coupling of adsorbates, or on stacked and multilayered heterostructures[4]. These systems have shown tunable electronic properties such as bandgap engineering[3], reversible metal–insulating transition[2,4] or supramolecular spintronics[5]. Tunable superconductivity is expected as well[6], but experimental realization is lacking. Here, we show experiments based on metal–graphene hybrid composites, enabling the tunable proximity coupling of an array of superconducting nanoparticles of tin onto a macroscopic graphene sheet. This material allows full electrical control of the superconductivity down to a strongly insulating state at low temperature. The observed gate control of superconductivity results from the combination of a proximity-induced superconductivity generated by the metallic nanoparticle array with the two-dimensional and tunable metallicity of graphene. The resulting hybrid material behaves, as a whole, like a granular superconductor showing universal transition threshold and localization of Cooper pairs in the insulating phase. This experiment sheds light on the emergence of superconductivity in inhomogeneous superconductors, and more generally, it demonstrates the potential of graphene as a versatile building block for the realization of superconducting materials.

Although intrinsic superconductivity in doped[6] graphene has been proposed, it has not yet been experimentally shown. However, graphene can carry supercurrent by means of the proximity effect[7], in which charge carriers in a non-superconducting material acquire superconducting correlations in the vicinity of a superconductor. In the present study, the proximity effect in graphene is not locally generated from the contacting electrodes, as is done in most mesoscale experiments[7], but rather by coupling its surface to a macroscopic 2D network of superconducting clusters[8]. As opposed to covalent functionalization of graphene, which strongly affects the density of states, non-covalent coupling of adsorbates on graphene is useful for designing materials with extended electronic functions, because the graphene keeps most of its exceptional electronic properties, while gaining others coming from the coupling elements (Fig. 1). Previous experiments involving decoration of metal clusters on exfoliated graphene have shown[9] that such a hybrid system can exhibit a gate-tunable Berezinsky–Kosterlitz–Thouless transition towards a fully two-dimensional (2D) superconducting state with a critical temperature related to the normal-state resistivity. In that experiment, the mean free path and the superconducting coherence length exceeded the average gap width separating neighbouring tin nanoparticles, resulting in homogeneous 2D superconductivity. Here, the main and crucial difference is the use of centimetre-scale graphene layers grown by chemical vapour deposition (CVD) instead of previously used micrometre-scaled exfoliated graphene.

The CVD-grown graphene used in this study has a significant electronic disorder that induces strong electron localization under 1 K (see characterization of bare graphene samples in Supplementary Figs S1 and S3 and Table S1). This results in a completely different behaviour: on gating the tin-decorated sample, one observes a superconductor-to-insulator transition (SIT). The SIT in 2D films of superconductors has been a very active field of research in the condensed-matter community for the past twenty years[10]. It is of interest not only for the study of quantum phase transitions[11], but also to understand how superconductivity emerges in high-T_c superconductors[12]. Recent advances in this field have involved the use of electric field to tune the SIT at constant disorder[12–14].

The samples, presented in Fig. 1, were fabricated by connecting CVD-grown graphene flakes transferred on oxidized silicon[15] (see Methods). A nominal thickness of 10 nm of tin was evaporated on the whole sample by thermal evaporation. Tin's dewetting (Fig. 1c) produces a self-assembled, non-percolating array of pancake-like nanoparticles[9] (Fig. 1a,b,d). The typical lateral size of a tin island is 80 nm, with a 13 nm gap between islands.

Samples have shown two kinds of behaviour depending on their room-temperature sheet resistance. Devices having the lowest sheet resistance (typically $\leq 10\,\mathrm{k\Omega/\square}$) showed superconductivity for all gate voltages with a gate-tunable transition temperature, similarly to what was reported for exfoliated samples[9]. Here, we will focus on the other type of devices, which exhibited a high sheet resistance ($\geq 15\,\mathrm{k\Omega/\square}$) at room temperature.

On cooling from room temperature down to 6 K, the resistivity increase ranges from 20% up to 100% at the charge neutrality point. This behaviour is consistent with the enhanced weak localization and electron–electron interactions expected in 2D metals. Just above the critical temperature of bulk tin ($T_c^{Sn} = 3.7$ K, black dotted line in Fig. 2a), a 10% resistance drop is observed (Fig. 2b), arising from superconducting fluctuations in graphene near the tin islands. Then a broad transition takes place, either towards a superconducting state at high electrostatic doping (for a gate voltage offset from the charge neutrality point $\Delta V_g > 45$ V), or towards an insulating state for voltages closer to the charge neutrality point ($\Delta V_g < 10$ V). In between these two gate voltage ranges, the resistance levels off at low temperatures (Fig. 2c), suggesting an intermediate metallic behaviour. On the superconducting side, the system follows an 'inverse Arrhenius law' $R \propto R_0 \exp(T/T_0)$, as already reported in quench-condensed granular films[16]. Significant fluctuations and levelling in the region just before superconductivity sets in (see Fig. 3, bump near $V_g = +10$ V) are indicative of a percolative

Institut Néel, CNRS-UJF-INP, BP 166, 38042 Grenoble cedex 9, France. *e-mail: bouchiat@grenoble.cnrs.fr.

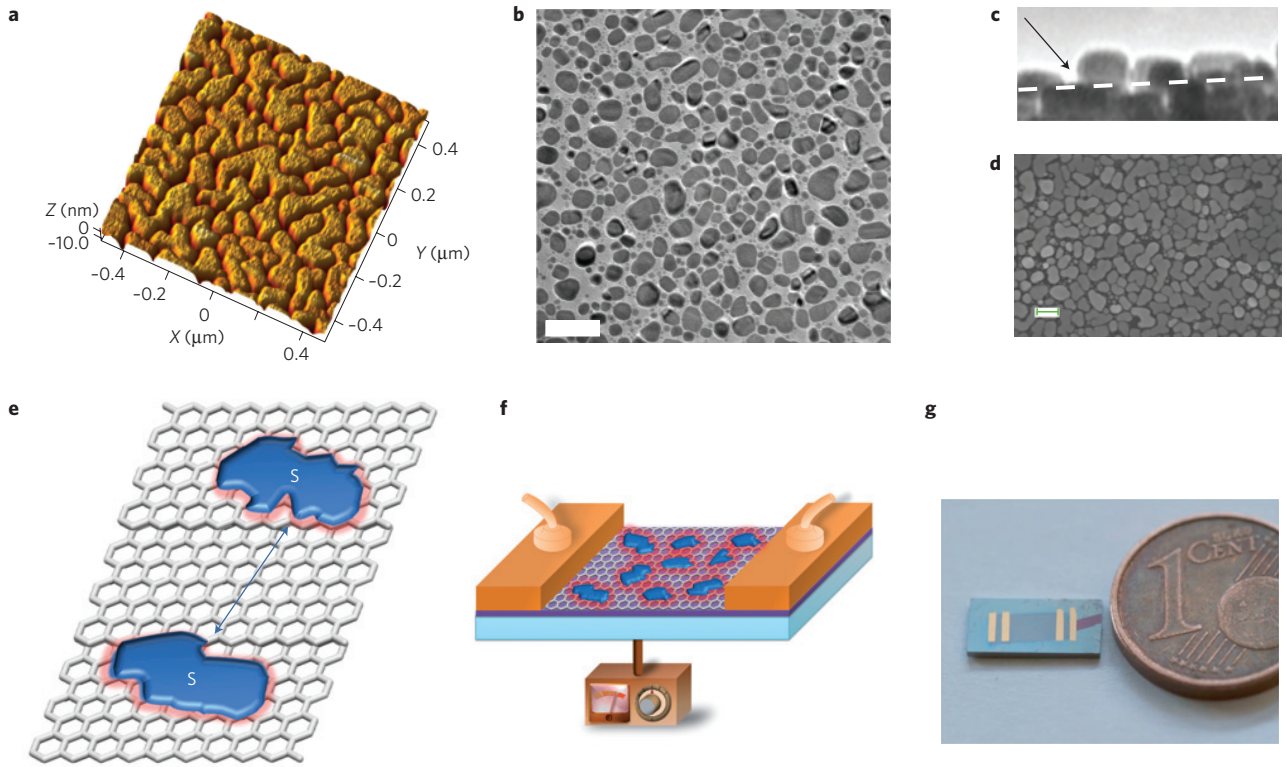

Figure 1 | Self-assembled graphene–tin nanohybrids. a, Atomic force micrograph of a 1 μm^2 area of the device, obtained by dewetting of an evaporated tin film of nominal thickness 10 nm. **b**, Transmission electron micrograph of the decorated sample showing the self-organized network of tin nanoparticles (scale bar, 200 nm) separated by clean graphene. **c**, Transmission electron micrograph of the sample transferred on a membrane and observed at a grazing angle (the dashed line corresponds to the graphene surface). The negative wetting angle of tin nanoparticles on graphene (black arrow) can be clearly seen. **d**, Scanning electron micrograph of the Sn nanoparticles network on graphene (scale bar, 300 nm). **e**,**f**, Sketches of the device. Changing the gate voltage modulates the extension of phase-coherent domains in graphene. S, superconductor. **g**, Photograph of the studied device. The dark region between the four electrodes is the decorated graphene sheet. The blue cast is due to the presence of tin nanoparticles on the whole surface. The enhanced contrast of the graphene sheet with respect to the silica sides comes from the difference of grain sizes and gaps between nanoparticles on graphene and on SiO_2.

behaviour. The amplitude of the critical current also supports this picture, as it was repetitively measured to be of the order of 1 μA, which corresponds to a critical current density of 5×10^{-4} A m^{-1}, a value 2,000 times smaller than the value found in samples made from exfoliated graphene[9] or clean CVD graphene.

Above 2 K, $R(T)$ curves at all gate voltages behave qualitatively the same. Reducing the temperature further, the curves near the charge neutrality point then reach a minimum at a gate-dependent temperature (red dotted line in Fig. 2b), below which they start to increase sharply. This re-entrant behaviour is reminiscent of what was observed in granular superconductors[17] or in Josephson junctions arrays[18]. Our system is indeed similar to a granular superconductor in which the role of the intergranular media is taken up by graphene. In such systems, the SIT is driven by the competition between the charging energy E_C of a superconducting island and the Josephson energy $E_J = (1/2)(h/4e^2)(\Delta/R_N)\tanh(\Delta/2k_BT)$, where R_N is the normal-state resistance of the junction. Dissipative degrees of freedom, such as quasiparticles[19] or capacitive coupling to a 2D electron gas[20] such as graphene[21], lead to renormalization of the charging energy. Here, the levelling-off of resistance in the intermediate 'metallic' regime is indicative of such dissipative processes[22]. Dissipation strength scales as R_N^{-1}, and R_N in turn depends on gate voltage and temperature, as can be seen by applying a magnetic field above the critical field (Supplementary Fig. S2). R_N thus tunes both energies (E_J and E_C) simultaneously, unlike previously considered situations[20,21]. Despite this complex dependence, the phase diagram of the SIT (Fig. 2d) shows that the boundary of the insulating region (red dotted line in Fig. 2b) can be related to a constant value of R_N.

Interestingly, when measuring resistance at constant temperature as a function of gate voltage (Fig. 3), one sees a crossing point at $V_g \cong -20$ V where the sheet resistance is of the order of $h/(2e)^2$, the pair quantum of resistance. The universal value of the critical resistance at the transition was predicted by the so-called dirty bosons model[23]. Around this transition, the resistance varies by more than seven orders of magnitude over a gate range of 40 V (corresponding to a carrier density change of 3×10^{12} cm^{-2}). This electrostatically driven transition shows a strongly insulating state, with exponential divergence of the resistance.

The magnetoresistance curves in the insulating and superconducting regions are presented in Fig. 4a and show a peak, both in the superconducting and in the insulating regions. Such a non-monotonic behaviour has been widely reported in superconducting thin films. By gating the sample, we observed a continuous crossover between different magnetoresistance regimes[24]. In the superconducting state (red curve in Fig. 4), the small resistance overshoot at intermediate magnetic field can be understood in terms of Galitski–Larkin correction to the conductivity[25]. The inflection point corresponds to the critical field expected in tin nanoparticles[26]. However, the behaviour in the insulating region (black curve in Fig. 4a) cannot be explained with perturbation theory. Here, the resistance at intermediate field ($B = 0.15$ T) is about 40 times higher than the resistance in the normal state ($B = 1$ T). Such huge effects have been reported in amorphous thin films[27,28], and have been explained[29] to stem from the underlying nature of superconductivity in amorphous thin films, which is inhomogeneous[30,31] near the transition. In a granular system, as

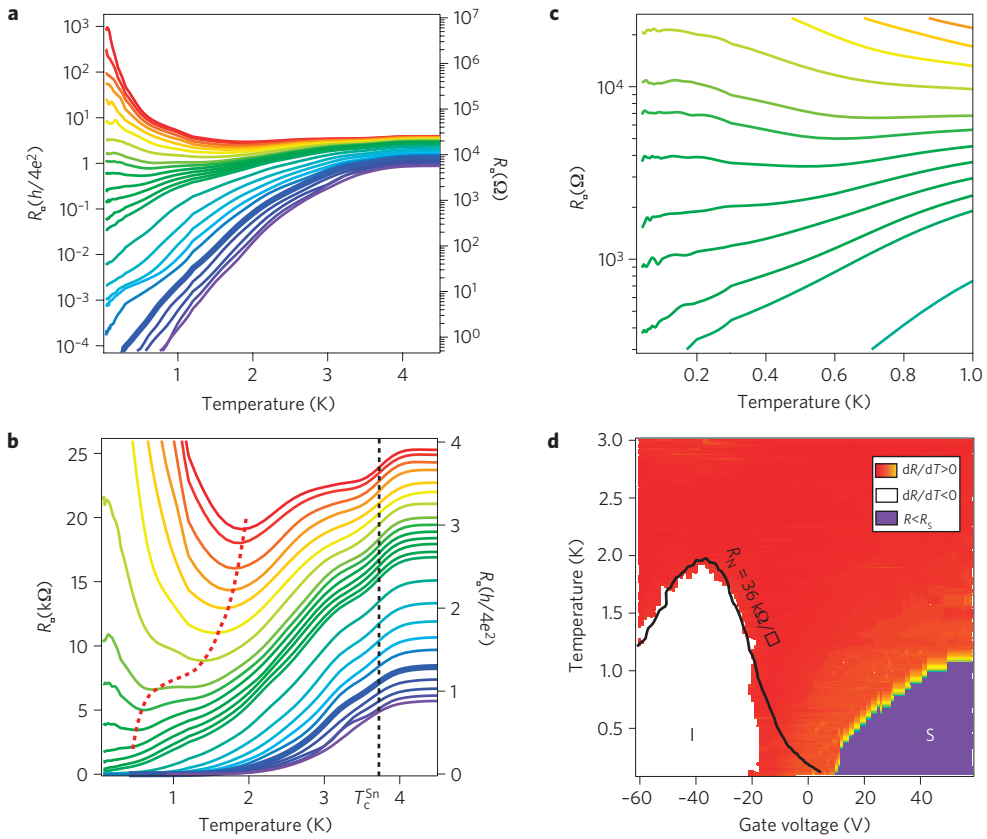

Figure 2 | Sheet resistance as a function of temperature for different gate voltages. a, Sheet resistance as a function of sample temperature for different gate voltages, plotted on a log scale. From top to bottom, voltage offsets from the charge neutrality point ($V_D = -36$ V, see Fig. 3) are $\Delta V_g = V_g - V_D = 0$, 3, 6, 8, 10, 12, 14, 16, 17, 18, 19, 20, 21, 22, 26, 31, 36, 41, 46, 56, 66, 76, 86, 96 V. **b**, The same data (lower part) plotted on a linear scale to emphasize the behaviour between 1 K and 4 K. The black dashed line indicates the critical temperature of tin. The red dashed line is a guide to the eye showing the minimum resistivity. **c**, Higher magnification of the critical region. **d**, Phase diagram of the SIT transition. $\log(\partial R/\partial T)$ versus gate voltage and temperature. I, insulating; S, superconducting. We call the region where R is below the noise floor ($R_S = 0.5\ \Omega$) superconducting. The black line is the iso-value of the normal-state resistivity obtained at $B = 1$ T (see Supplementary Fig. S2) that appeared the closest to the border between the two states.

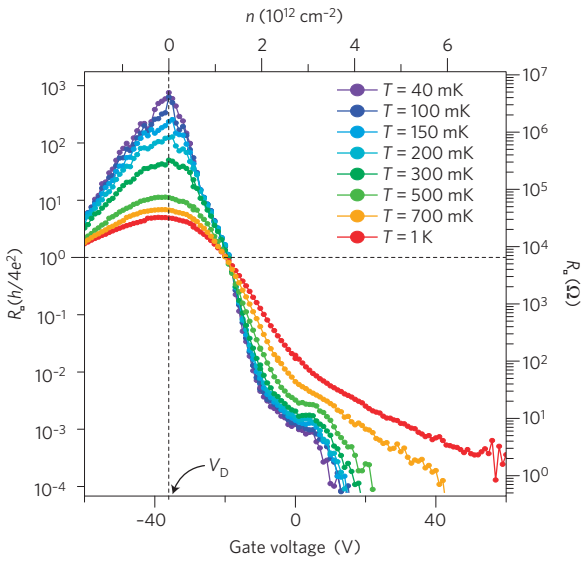

Figure 3 | Sheet resistance as a function of gate voltage for different temperatures. Gate-voltage dependence of sheet resistance for the lowest temperatures. The vertical dotted line indicates the charge neutrality point. The horizontal one indicates the quantum of resistance for Cooper pairs $R_\square = h/4e^2$ (top axis: carrier density calculated using the gate capacitance per unit area for 285 nm of SiO_2 $C_{bg} = 121\ \mu F\ m^{-2}$).

grains of different sizes have different critical fields, there exists an intermediate field where half of the grains are superconducting and the other half are normal. Normal–superconducting junctions can prevent percolation as they provide barriers for both quasiparticles and Cooper pairs. As we move away from the insulating region (by increasing ΔV_g), the resistivity maximum is shifted towards higher magnetic fields. This indicates that islands with the smaller critical fields ($B_C \approx 0.15$ T) play a crucial role in the percolation process, whereas deep in the superconducting region, coupling is established directly between other islands.

Finally, the temperature dependence of the system when biased at $\Delta V_g = 0$ and for $B = 0.15$ T (that is, in the region where Cooper pairs are localized) does not quite follow the activation law predicted previously[29]. Instead it shows an Efros–Schklovsky-like behaviour $T \propto \exp(T_1/T)^{1/2}$ with an activation energy $T_1 = 32.6$ K (Fig. 4b), suggesting that Coulomb interactions may play an important role in the transport.

Going back to the gate-induced SIT, Fig. 5 shows how the data can be interpreted as a quantum phase transition[11], using finite-size scaling. The voltage range around the critical gate voltage $V_{g_c} = -20$ V was chosen to be the largest possible (± 6 V) while still retaining a universal exponent on both (insulating and superconducting) sides. Below 600 mK, the field effect at the transition shows a significant shift from the universal behaviour. The presence of puddles of normal electrons in the graphene sheet, which are sources of gapless excitations[21], provides a dissipative environment. The system becomes more coupled at low temperatures to

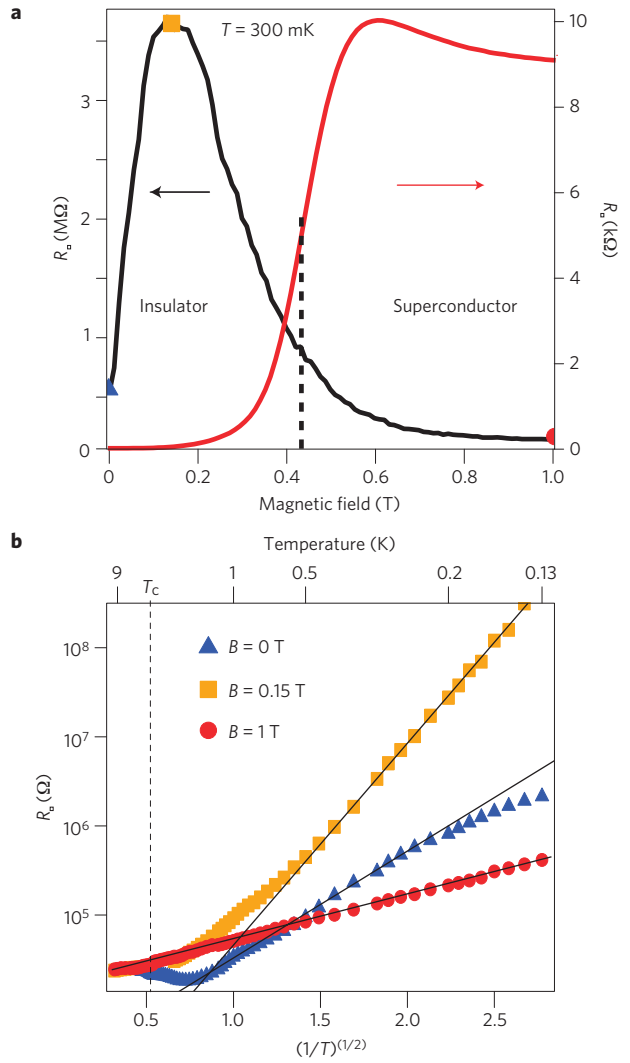

Figure 4 | Localization of Cooper pairs under a magnetic field. a, Sheet resistance as a function of magnetic field, measured at $T = 300$ mK. The black curve shows the magnetoresistance at the charge neutrality point. The red curve has been measured deep in the superconducting region. **b**, Temperature dependence of the sheet resistance at three different magnetic fields (indicated in the upper panel). The black lines are fits to the Efros–Schklovsky law, giving the following activation temperatures: $T_1 = 7.8$ K, $T_1' = 32.6$ K and $T_1'' = 2.5$ K for $B = 0$ T, 0.15 T and 1 T, respectively.

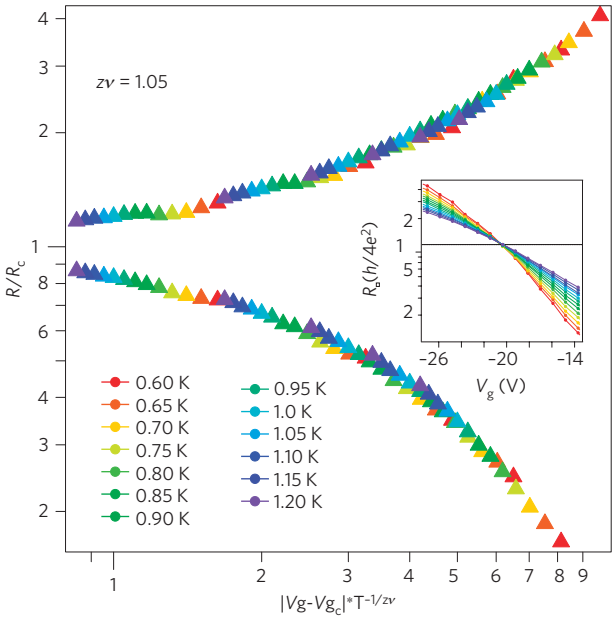

Figure 5 | Universal scaling of the transition. Finite-size scaling analysis of the quantum phase transition, using data from Fig. 3. The best collapse was found using $\nu z = 1.05 \pm 0.05$. Inset, subset of the data used for the scaling: 0.6 K $< T <$ 1.3 K and a gate voltage interval of ± 6 V around the critical point $V_{g_c} = -20$ V.

dissipative degrees of freedom, leading to a breakdown of the universal behaviour, as already observed in experiments involving MoGe films[22]. However, above 600 mK, the critical resistance lies very close to the value predicted by the dirty bosons model: $R_C/R_Q \cong 1.2$, $R_Q = h/4e^2$, which is an indication that we are in the regime of low dissipation, where the dynamical critical exponent z is still equal to 1 (ref. 32). The exponent $z\nu$ has been evaluated using the two methods described in ref. 33. The first method is to multiply each curve by the factor t yielding the best collapse to the first curve, and then fitting t to $T^{-z\nu}$. The second method is to take the slope of $\log[(\partial R/\partial V_g)_{V_{g_c}}]$ versus $\log(T^{-1})$. The first method (shown in Fig. 5) leads to $z\nu = 1.05 \pm 0.10$ whereas the second method gives a value of $z\nu = 1.18 \pm 0.02$ (Supplementary Fig. S4). The second method is probably more accurate, as it is based on data that are taken within the critical region. This value is close to other reported values of $z\nu$ in thickness-tuned transition in Bi (ref. 33). Note that this exponent differs from the expected exponent for classical percolation in 2D ($z\nu = 4/3$). It is instead in good agreement with recent theoretical developments on the superfluid transition in disordered 2D bosonic systems[34], which can be understood as the percolation of phase-coherent domains into a macroscopic superfluid.

Unlike previously reported gate-induced SITs that either showed a partial SIT transition towards a weakly localized metal[12,13,35] or involved ionic gating, which freezes at low temperatures[14], tin-decorated CVD graphene can be gated continuously at low temperatures with a very strong transconductance (Fig. 3). This could have application, for example in transition-edge particle detectors. The recently demonstrated metal–insulator transition in ultraclean graphene samples[4] also opens exciting new perspectives to probe the SIT in the opposite limit of very low disorder. The present experiment paves the way to the realization of more complex graphene-based hybrid materials where graphene acts as a tunable medium or an adjustable environment that controls the establishment of long-range electronic orders, such as superconductivity or ferromagnetism. This experiment sheds light on the emergence of superconductivity in inhomogeneous superconductors, and demonstrates the potential of graphene as a versatile substrate for the realization of hybrid superconducting materials.

Methods

Sample preparation. Graphene is grown using a CVD technique on copper foils (typically 25 μm thick, from Alfa-Aesar) following the methods described previously[15]. During the growth, a flow of methane (CH_4) provides the carbon feedstock, and forming gas (H_2/Ar 1:9) limits the reaction and only a single layer of graphene is obtained. After growth, the graphene is protected with a support layer of 1-μm-thick polymethyl methacrylate (PMMA), and copper is etched away using a solution of 0.2 g ml^{-1} sodium persulphate ($Na_2S_2O_8$). The graphene remains attached to PMMA and floats in the solution. It is then carefully transferred onto a wafer of degenerately doped oxidized silicon and PMMA is removed using an acetone wash followed by thermal annealing at 380 °C for 1 h under an argon atmosphere. Tin is deposited on the whole sample using room-temperature Joule evaporation. Pd/Au electrodes are subsequently deposited using a millimetre-scaled metal foil stencil mask in a four-probe geometry aligned on top of the graphene sheet. Supplementary Fig. S1 shows a typical sample after fabrication. The fabricated samples were about 5 mm in length and 3 mm in width, sizes that could not previously be obtained using exfoliated graphene. Such a macroscopic sample allowed us to get mesoscopic effects such as universal

conductance fluctuations to be averaged out, which is crucial when studying how the phase transition scales.

Several samples were measured, and the number of graphene layers was varied (from 1 to 3), as well as the thickness of tin (8–20 nm). However, we did not see a direct correlation between these parameters and the behaviour of the device. We could relate it only to the normal-state sheet resistance of graphene. Only graphene showing a high sheet resistance at room temperature ($>15\,k\Omega$) would behave as an insulator below the tin's superconducting transition temperature (3.7 K). The other samples behaved like the ones studied in ref. 9, showing much higher critical current density and a gate-tunable Berezinsky–Kozterlitz–Thouless transition towards a superconducting state at all gate voltages.

Measurement set-up. The sample was thermally anchored to the mixing chamber of a $^3He/^4He$ dilution cryostat and connected to highly filtered measurement lines. The set-up allowed the temperature to be continuously varied between 10 K and 0.03 K. The differential resistance was recorded using a lock-in amplifier operated in a four-probe configuration at frequencies between 9 Hz and 37 Hz, with an excitation current of 1 nA. In the high-impedance state, a two-probe, voltage-biased configuration was used with a Keithley 6430 electrometer or a Femto current-to-voltage converter to record the current.

Received 23 January 2012; accepted 17 April 2012; published online 20 May 2012

References

1. Geim, A. K. & Novoselov, K. S. The rise of graphene. *Nature Mater.* **6,** 183–191 (2007).
2. Elias, D. C. *et al.* Control of graphene's properties by reversible hydrogenation: evidence for graphane. *Science* **323,** 610–613 (2009).
3. Kozlov, S. M., Vines, F. & Görling, A. Bandgap engineering of graphene by physisorbed adsorbates. *Adv. Mater.* **23,** 2638–2643 (2011).
4. Ponomarenko, A. L. *et al.* Tunable metal-insulator transition in double-layer graphene heterostructure. *Nature Phys.* **7,** 958–961 (2011).
5. Candini, A. *et al.* Graphene spintronic devices with molecular nanomagnets. *Nano Lett.* **11,** 2634–2639 (2011).
6. Uchoa, B. & Castro Neto, A-H. Superconducting states of pure and doped graphene. *Phys. Rev. Lett.* **98,** 146801 (2007).
7. Heersche, H. B., Jarillo-Herrero, P., Oostinga, J. B., Vandersypen, L. & Morpurgo, A. F. Bipolar supercurrent in graphene. *Nature* **446,** 56–59 (2007).
8. Feigel'man, M. V., Skvortsov, M. A. & Tikhonov, K. S. Proximity-induced superconductivity in graphene. *JETP Lett.* **88,** 747–751 (2008).
9. Kessler, B. M., Girit, C. Ö., Zettl, A. & Bouchiat, V. Tunable superconducting phase transition in metal-decorated graphene sheets. *Phys. Rev. Lett.* **104,** 047001 (2010).
10. Goldman, A. M. & Markovic, N. Superconductor–insulator transitions in the two-dimensional limit. *Phys. Today* **51,** 39–43 (November 1998).
11. Sondhi, S. L., Girvin, S. M., Carini, J. P. & Shahar, D. Continuous quantum phase transitions. *Rev. Mod. Phys.* **69,** 315–333 (1997).
12. Bollinger, A. T. *et al.* Superconductor–insulator transition in $La_{2x}Sr_xCuO_4$ at the pair quantum resistance. *Nature* **472,** 458–460 (2011).
13. Parendo, K. A. *et al.* Electrostatic tuning of the superconductor–insulator transition in two dimensions. *Phys. Rev. Lett.* **94,** 197004 (2005).
14. Leng, X., Garcia-Barriocanal, J., Bose, S., Lee, Y. & Goldman, A. M. Electrostatic control of the evolution from a superconducting phase to an insulating phase in ultrathin $YBa_2Cu_3O_{7-x}$ films. *Phys. Rev. Lett.* **107,** 027001 (2011).
15. Li, X. S. *et al.* Large-area synthesis of high-quality and uniform graphene films on copper foils. *Science* **324,** 1312–1314 (2009).
16. Frydman, A., Naaman, O. & Dynes, R. C. Universal transport in two-dimensional granular superconductors. *Phys. Rev. B* **66,** 052509 (2002).
17. Jaeger, H. M., Haviland, D. B., Orr, B. G. & Goldman, A. M. Onset of superconductivity in ultrathin granular metal films. *Phys. Rev. B* **40,** 182–196 (1989).
18. Van der Zant, H. S. J., Elion, W. J., Geerlings, L. J. & Mooij, J. E. Quantum phase transitions in two dimensions: Experiments in Josephson-junction arrays. *Phys. Rev. B* **54,** 10081–10093 (1996).
19. Chakravarty, S., Kivelson, S., Zimanyi, G. T. & Halperin, B. I. Effect of quasiparticle tunneling on quantum-phase fluctuations and the onset of superconductivity in granular films. *Phys. Rev. B* **35,** 7256–7259 (1987).
20. Rimberg, A. J. *et al.* Dissipation-driven superconductor–insulator transition in a two-dimensional Josephson-junction array. *Phys. Rev. Lett.* **78,** 2632–2635 (1997).
21. Lutchyn, R. M., Galitski, V., Refael, G. & Das Sarma, S. Dissipation-driven quantum phase transition in superconductor-graphene systems. *Phys. Rev. Lett.* **101,** 106402 (2008).
22. Mason, N. & Kapitulnik, A. Dissipation effects on the superconductor–insulator transition in 2D superconductors. *Phys. Rev. Lett.* **82,** 5341–5344 (1999).
23. Fisher, M. P. A., Grinstein, G. & Girvin, S. M. Presence of quantum diffusion in two dimensions: Universal resistance at the superconductor–insulator transition. *Phys. Rev. Lett.* **64,** 587–590 (1990).
24. Steiner, M. A., Boebinger, G. & Kapitulnik, A. Possible field-tuned superconductor–insulator transition in high-T_c superconductors: Implications for pairing at high magnetic fields. *Phys. Rev. Lett.* **94,** 107008 (2005).
25. Galitski, V. M. & Larkin, A. I. Superconducting fluctuations at low temperature. *Phys. Rev. B* **63,** 174506 (2001).
26. Wang, X-L., Feygenson, M., Aronson, M. C. & Han, W-Q. Sn/SnO_x core-shell nanospheres: Synthesis, anode performance in Li–Ion batteries, and superconductivity. *J. Phys. Chem. C* **114,** 14697–14703 (2010).
27. Nguyen, H. Q. *et al.* Observation of giant positive magnetoresistance in a Cooper pair insulator. *Phys. Rev. Lett.* **103,** 157001 (2009).
28. Baturina, T. I. *et al.* Localized superconductivity in the quantum-critical region of the disorder-driven superconductor–insulator transition in TiN thin films. *Phys. Rev. Lett.* **99,** 257003 (2007).
29. Beloborodov, I. S., Fominov, Ya. V., Lopatin, A. V. & Vinokur, V. M. Insulating state of granular superconductors in a strong-coupling regime. *Phys. Rev. B* **74,** 014502 (2006).
30. Sacépé, B. *et al.* Disorder-induced inhomogeneities of the superconducting state close to the superconductor–insulator transition. *Phys. Rev. Lett.* **101,** 157006 (2008).
31. Sacépé, B. *et al.* Localization of preformed Cooper pairs in disordered superconductors. *Nature Phys.* **7,** 239–244 (2011).
32. Wagenblast, K-H., van Otterlo, A., Schön, G. & Zimanyi, G. T. New universality class at the superconductor–insulator transition. *Phys. Rev. Lett.* **78,** 1779–1782 (1997).
33. Markovic, N., Christiansen, C., Mack, A. M., Huber, W. H. & Goldman, A. M. Superconductor–insulator transition in two dimensions. *Phys. Rev. B* **60,** 4320–4328 (1999).
34. Iyer, S., Pekker, D. & Refael, G. A Mott glass to superfluid transition for random bosons in two dimensions. *Phys. Rev. B* **85,** 094202 (2012).
35. Caviglia, A. D. *et al.* Electric field control of the $LaAlO_3/SrTiO_3$ interface ground state. *Nature* **456,** 624–627 (2008).

Acknowledgements

This work is partially supported by ANR-BLANC SuperGraph, ERC Advanced Grant MolNanoSpin No. 226558 and the Cible programme from Région Rhone-Alpes. Samples were fabricated at the NANOFAB facility of the Néel Institute, the support team of which is gratefully acknowledged. We thank H. Arjmandi-Tash, N. Bendiab, H. Bouchiat, C. Chapelier, J. Coraux, M. V. Feigel'man, Ç.Ö. Girit, B. M. Kessler, L. Marty, A. Reserbat-Plantey, B. Sacépé, V. Sessi, W. Wernsdorfer and A. Zettl for help and stimulating discussions.

Author contributions

V.B. and A.A. conceived the experiments, Z.H. grew the graphene, A.A. and Z.H. fabricated the samples and carried out the measurements, A.A. and V.B. analysed the data and wrote the paper.

Additional information

The authors declare no competing financial interests. Supplementary information accompanies this paper on www.nature.com/naturematerials. Reprints and permissions information is available online at www.nature.com/reprints. Correspondence and requests for materials should be addressed to V.B.